Polyhedron 65 (2013) 170–180

Contents lists available at ScienceDirect

Polyhedron

journal homepage: www.elsevier.com/locate/poly

Studies on phenylmercury(II) complexes of nitrogen–sulfur ligands: Synthesis, spectral, structural characterization, TD-DFT and photoluminescent properties

A. Bharti [a], P. Bharati [a], Ram Dulare [c], M.K. Bharty [a,*], Dheeraj K. Singh [b], N.K. Singh [a,*]

[a] Department of Chemistry, Banaras Hindu University, Varanasi 221005, India
[b] Department of Physics, Banaras Hindu University, Varanasi 221005, India
[c] Department of Chemistry, P.G. College, Ghazipur, India

ARTICLE INFO

Article history:
Received 1 April 2013
Accepted 4 August 2013
Available online 20 August 2013

Keywords:
Phenylmercury(II) complexes
Thiadiazole complex
Carbodithioate complex
Secondary interactions
Hydrogen bonding
Supramolecular architecture

ABSTRACT

The reactions of phenylmercury(II) acetate with N-phenyl-5-(pyridin-4-yl)-1,3,4-thiadiazol-2-amine (Hppt) (**1**) and potassium N(4-methylpiperazine)-1-carbodithioate [K(mpcdt)] yielded [PhHg(ppt)] (**2**) and [PhHg(mpcdt)] (**3**). The complexes have been characterized by elemental analyses, IR, UV–Vis, ^{1}H and ^{13}C NMR spectroscopy. The ligand Hppt (**1**)- and complexes **2** and **3** crystallize in the triclinic, monoclinic and orthorhombic system, space group $P\bar{1}$, $C\,2/c$ and *Pbca*, respectively. The crystal X-ray studies revealed that complexes **2** and **3** both form a one dimensional metal–organic structure, with a linear N–Hg–Ph and S–Hg–Ph core respectively. The most noteworthy features in complex **2** is that the ligand bound phenylmercury cation is stabilized via intramolecular as well as intermolecular weak Hg···N secondary interactions. Crystal structure of complex **2** is also stabilized via weak π···π and C–H···π interactions. The crystal structure of complex **3** is stabilized by intermolecular/intramolecular Hg···S interactions and C–H···π interactions. The ligands Hppt and [K(mpcdt)] exhibit green emissions and complex **2** shows photoluminescence due to the presence of Hg···N interactions, whilst complex **3** does not show photoluminescence because Hg···S interactions show quenching behaviour in the solid state. The solution state photoluminescence properties of complex **2** indicate that intermolecular as well as intramolecular Hg···N interactions persist even in very dilute solution. The geometrical optimization of Hppt (**1**), [K(mpcdt)] and complexes **2** and **3** was calculated in the gas phase using density functional theory (DFT) with the B3LYP hybrid functional, and was used to predict their molecular properties. The electronic excitation energies and intensities of the six lowest-energy spin allowed transitions were calculated using time dependent density functional theory (TD-DFT).

1. Introduction

Organomercury(II) cations have a high affinity for the sulfur donor atoms present in proteins, peptides and amino acids [1–3]. Hg(II) has an extremely high affinity for complexation with sulfhydryl groups in the blood and tissues of humans where it is bound by cysteine-containing peptides and proteins. Metal complexes with nitrogen–sulfur rich ligands are very interesting from the viewpoint of their electrical conductivity, molecular magnetism, electrochemical properties, biological processes and optoelectronic properties [4]. Phenylmercury(II) compounds have gained significant attention because of their importance in the preparation of other organometallics as intermediates in organic chemistry and their relevance to mercury detoxification [5,6]. Phenylmercury(II) carbodithioates have been found to be extremely versatile groups for the construction of supramolecular arrays, exhibiting luminescence properties and they are also used in dye sensitized solar cells [7]. Phenylmercury(II) carbodithioate complexes show a bulkiness of the pendant group in the carbodithioate part of the compound, which plays an important role in the construction of the supramolecular framework through Hg···S interactions. Weak intermolecular as well as intramolecular Hg···N secondary interactions and other non-covalent interactions can determine the solution state luminescent properties of organometallic compounds [8]. The thiohydantoin ring coordinates to the phenylmercury cation mainly via its deprotonated N–H group, resulting in a very short Hg···N distance, while both intermolecular and intramolecular Hg···S distances are rather long [9]. Two types of ligands were chosen to stabilize the organomercury(II) cation. The first of these was N-phenyl-5-(pyridine-4-yl)-1,3,4-thiadiazol-2-amine because it is a conjugate system possessing a nitrogen donor and its complex may be stabilized via intermolecular as well as intramolecular

* Corresponding authors. Tel.: +91 542 6702452.
E-mail addresses: mkbharty@bhu.ac.in (M.K. Bharty), singhnk_bhu@yahoo.com (N.K. Singh).

0277-5387/$ - see front matter © 2013 Elsevier Ltd. All rights reserved.
http://dx.doi.org/10.1016/j.poly.2013.08.032

Hg···N interactions, capable of enhancing photoluminescent properties. The other ligand, N(4-methylpiperazine)-1-carbodithioate, has no conjugate system, it is a sulfur donor and the complex may be stabilized via intermolecular and intramolecular Hg···S interactions, which exhibit photoluminescent quenching properties. In view of the above, we report herein the synthesis, spectral, X-ray crystal data, time dependent density functional theory, electrostatic potential mapping and photoluminescent studies of the phenylmercury(II) complexes [PhHg(ppt)] (**2**) and [PhHg(mpcdt)] (**3**), derived from N-phenyl-5-(pyridine-4-yl)-1,3,4-thiadiazol-2-amine and N(4-methylpiperazine)-1-carbodithioate, respectively.

2. Experimental

2.1. Materials and methods

Commercial reagents were used without further purification and all experiments were carried out in an open atmosphere at room temperature. Phenyl isothiocyanate, 4-methylpiperazine, isonicotinic acid hydrazide (Sigma–Aldrich), CS_2 (SD Fine Chemicals) and KOH (Qualigens) were used as received. The solvents were dried and distilled before use following the standard procedures. Carbon, hydrogen, nitrogen and sulfur contents were estimated on an Elementar Vario EL III Carlo Erbo 1108. The electronic spectra were recorded on a SHIMADZU 1700 UV–Vis spectrophotometer. IR spectra were recorded in the 4000–400 cm^{-1} region as KBr pellets on a Varian Excalibur 3100 FT-IR spectrophotometer. ^1H and ^{13}C NMR spectra were recorded in DMSO-d_6 on a JEOL AL300 FT NMR spectrometer using TMS as an internal reference.

2.2. Synthesis of N-phenyl-5-(pyridine-4-yl)-1,3,4-thiadiazol-2-amine (Hppt) (*1*)

A mixture of isonicotinic acid hydrazide (2.74 g, 20 mmol) and phenyl isothiocyanate (2.4 ml, 20 mmol) in benzene was refluxed for 8 h at 80 °C. On cooling the mixture, a white precipitate of 1-isonicotinoyl-4-phenyl thiosemicarbazide was obtained which was filtered off, washed with water and diethyl ether, air dried and crystallized from ethanol. The above prepared 1-isonicotinoyl-4-phenyl thiosemicarbazide (2.72 g, 10 mmol) was added slowly to 10 ml conc. H_2SO_4 and stirred for 2 h at low temperature. The mixture was poured over crushed ice and the precipitated solid was filtered off, washed twice with cold water and dried. Yellow crystals of Hppt (**1**) suitable for X-ray analysis were obtained by slow evaporation of the methanol solution over 15 days. Yield: 85%. *Anal.* Found: C, 61.35; H, 3.96; N, 22.20; S, 12.65%. Calc. for $C_{13}H_{10}N_4S$ (254.31): C, 61.34; H, 3.93; N, 22.02; S, 12.58%; m.p. 140 °C; IR (KBr, cm^{-1}): 3003m ν(NH), 1484m ν(C=N), 685 (pyridine), 826 (phenyl). ^1H NMR (DMSO-d_6, δ, ppm): [8.86 (2H), 8.19 (2H)] pyridine; [7.60 (2H), 7.37 (1H), 7.11 (2H)] phenyl; 4.84 (1H, NH). ^{13}C NMR (DMSO-d_6, δ, ppm): [146.42 C(4,7), 140.01 C(3), 122.93 C(5,6)] pyridine; [141.58 C(8), 129.30 C(10,12), 122.93 C(11), 122.07 C(9,13)] phenyl; [174.62 C(1), 153.88 C(2)] thiadiazole carbons of Hppt. UV–Vis [λ_{max}, DMSO, nm]: 319, 334, 350. The synthesis of the ligand Hppt has been reported [10] but its characterization by single crystal X-ray was not available.

2.3. Synthesis of potassium N′(4-methylpiperazine)-1-carbodithioate [K(mpcdt)]

The potassium N′(4-methylpiperazine)-1-carbodithioate was prepared by the addition of CS_2 (1.5 ml, 20 mmol) dropwise to a suspension of 4-methylpiperazine (2.20 ml, 20 mmol) in methanol (20 ml) in the presence of potassium hydroxide (1.2 g, 20 mmol). The reaction mixture was stirred continuously for 40 min and the separated white solid potassium N′(4-methylpiperazine)-1-carbodithioate [K(mpcdt)] was filtered, washed with EtOH and air dried. Yield: 70%; m.p. 205 °C. *Anal.* Found: C, 33.50; H, 5.13; N, 13.08; S, 29.80%. Calc. for $C_6H_{11}N_2S_2K$ (215.00): C, 33.48; H, 5.11; N, 13.02; S, 29.76%. IR (KBr, ν cm^{-1}): ν(C=N) 1469, ν(C=S) 970. ^1H NMR (DMSO-d_6, δ, ppm): 2.20–3.06 (m, 8H, CH_2), 4.38 (s, 3H, CH_3). ^{13}C NMR (DMSO-d_6, δ, ppm): 200.10 (C=S), 154.05 (C–N), 51.80–54.25 (CH_2), 45.25 (CH_3). UV–Vis [λ_{max}, DMSO, nm]: 268, 288.

2.4. Synthesis of [PhHg(ppt)] (*2*)

A methanol–chloroform solution of Hppt (0.254 g, 1 mmol) was added to a methanol–chloroform solution of phenylmercury(II) acetate (0.336 g, 1 mmol) and the solution was stirred slowly for 4 h. The resulting clear yellow solution was filtered off and kept for crystallization at room temperature. Single crystals suitable for X-ray analysis were obtained on slow evaporation of the solvent over 21 days. Yield: 55%; m.p. 215 °C. *Anal.* Found: C, 42.91; H, 2.60; N, 10.51; S, 6.59%. Calc. for $C_{19}H_{14}HgN_4S$ (531.00): C, 42.93; H, 2.63; N, 10.54; S, 6.02%. IR (KBr, cm^{-1}): 1484m ν(C=N), 685 (pyridine), 826 (phenyl). ^1H NMR (DMSO-d_6, δ, ppm): [8.86 (2H), 8.19 (2H)] pyridine; [7.60 (2H), 7.37 (1H), 7.11 (2H)] phenyl. ^{13}C NMR (DMSO-d_6, δ, ppm): [146.05 C(4,7), 138.81 C(3), 123.30 C(5,6)] pyridine; [138.60 C(8), 129.44 C(10,12), 120.63 C(11), 120.11 C(9,13)] phenyl; [174.44 C(1), 150.72 C(2)] thiadiazole carbons of Hppt. UV–Vis [λ_{max}, DMSO, nm]: 254, 263, 351 (Scheme 1).

2.5. Synthesis of [PhHg(mpcdt)] (*3*)

A solution of [K(mpcdt)] (0.215 g, 1 mmol) in MeOH (10 ml) was added to a MeOH–$CHCl_3$ solution (10 ml) of phenylmercury(II) acetate (0.336 g, 1 mmol). This mixture was stirred continuously for 5 h at room temperature. The resulting clear yellow solution was filtered off and kept for crystallization. White single crystals of **3** suitable for X-ray analysis were obtained by slow evaporation of the above solution over a period of 22 days. Yield: 50%; m.p. 360 °C. *Anal.* Found: C, 31.72; H, 4.50; N, 6.21; S, 14.18%. Calc. for $C_{12}H_{16}HgN_2S_2$ (453.00): C, 31.78; H, 3.53; N, 6.18; S, 14.12%. IR (ν cm^{-1}, KBr): 1464 ν(C–N), 912 ν(C–S), 443 ν(Hg–S). ^1H NMR ($CDCl_3$, δ, ppm): 2.32–2.52 (m, 8H, CH_2), 4.10 (s, 3H, CH_3) 7.11–7.67 (m, 5H, aromatic protons). ^{13}C NMR (DMSO-d_6, δ, ppm): 202.10 (C=S), 128.32–154.36 (phenyl ring), 51.80–54.25 (CH_2), 45.25 (CH_3) (Scheme 2). UV–Vis [λ_{max}, DMSO, nm]: 258, 297.

2.6. X-ray crystallography

Crystals suitable for X-ray analyses of compounds **1**, **2** and **3** were grown at room temperature. The crystal data were collected on an Oxford Gemini diffractometer equipped with a CrysAlis CCD software using a graphite monochromated Mo Kα (λ = 0.71073 Å) radiation source at 293 K for **1**, **2** and **3**. A multi-scan absorption correction was applied to the X-ray data collection for all the compounds. The structures were solved by direct methods (SHELXS-08) and refined against all data by full matrix least-square on F^2 using anisotropic displacement parameters for all non-hydrogen atoms. All hydrogen atoms were included in the refinement at geometrically ideal positions and refined with a riding model [11]. The MERCURY package and the ORTEP-3 for Windows program were used for generating the structures [12,13].

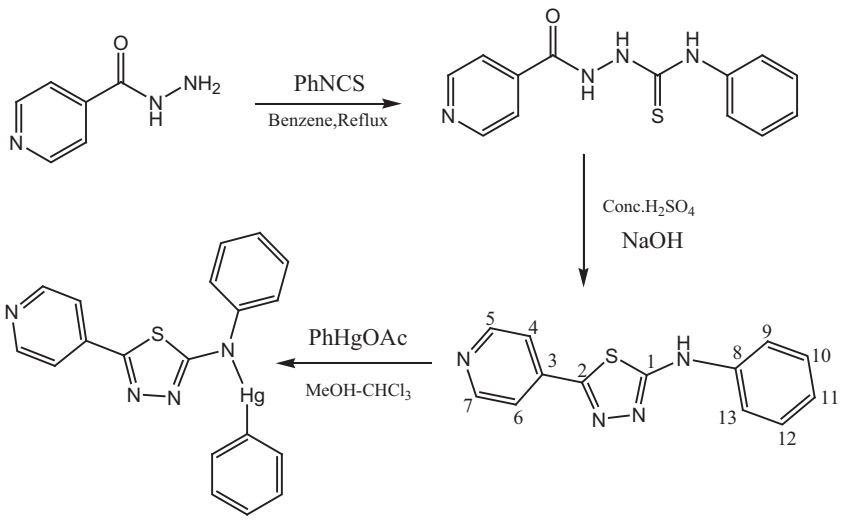

Scheme 1. Synthesis of N-phenyl-5-(pyridine-4-yl)-1,3,4-thiadiazol-2-amine (**1**) and its PhHg(II) complex **2**.

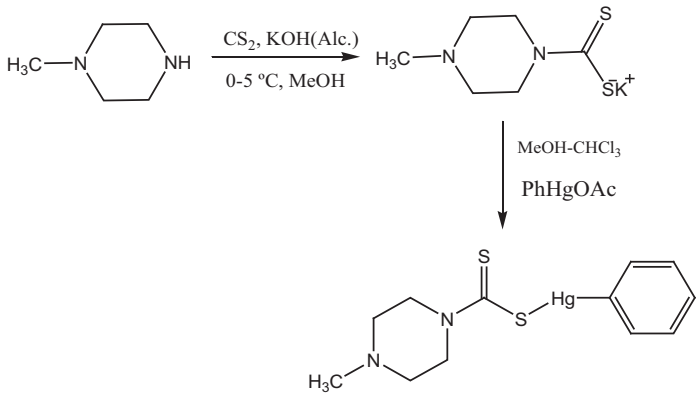

Scheme 2. Synthesis of potassium N-(4-methylpiperazine)-1-carbodithioate (mpcdt) and its PhHg(II) complex **3**.

3. Results and discussion

3.1. General aspects

The ligand N-phenyl-5-(pyridine-4-yl)-1,3,4-thiadiazol-2-amine was synthesized by the cyclization of 1-isonicotinoyl-4-phenyl thiosemicarbazide in the presence of strong acid followed by careful neutralization with NaOH solution at the low temperature of 0–5 °C. The methanol–chloroform solution of the ligand N-phenyl-5-(pyridine-4-yl)-1,3,4-thiadiazol-2-amine (Hppt) (**1**) reacts with phenylmercury(II) acetate to form a yellow coloured clear solution which gives colourless crystals of the complex [PhHg(ppt)] (**2**), whereas a methanol–chloroform solution of phenylmercury(II) acetate on reaction with a methanolic suspension of potassium N′(4-methylpiperazine)-1-carbodithioate yields a colourless clear solution which forms single crystals of the complex [PhHg(mpcdt)] (**3**). The ligands and complexes are stabilized via various types of interactions, such as C–H···π, hydrogen bonding and weak Hg···S or Hg···N secondary interactions. All the compounds are air-stable and were characterized by elemental analyses, IR, ^{1}H and ^{13}C NMR spectroscopy, and their structural elucidation is achieved by single crystal X-ray diffraction techniques. Complexes **2** and **3** are insoluble in methanol, ethanol and chloroform but are soluble in DMSO, and they melt at 215 and 360 °C, respectively.

3.2. Spectroscopy

The IR spectrum of the ligand N-phenyl-5-(pyridine-4-yl)-1,3,4-thiadiazol-2-amine (Hppt) (**1**) in KBr shows absorption bands at 3003, 1484, 1070 and 829 cm^{-1} due to the stretching modes of N–H, C=N, N–N and C–S, respectively. In the complex [PhHg(ppt)] (**2**), the disappearance of the NH band and the appearance of a new band at 485 cm^{-1} due to an M–N stretching vibration [14] indicates that the phenylmercury cation is bonded through the deprotonated NH group of the ligand. The IR spectrum of potassium N′(4-methylpiperazine)-1-carbodithioate in KBr shows absorptions due to the stretching modes of ν(C–N) and ν(C=S) at 1469 and 970 cm^{-1}, respectively. Whilst in the complex [PhHg(mpcdt)] (**3**), the appearance of a ν(C=S) band at 912 cm^{-1} indicates that the carbodithioate sulfur is involved in bonding with the phenylmercury cation. All the compounds show well resolved ^{1}H NMR signals. The ^{1}H NMR spectrum of Hppt shows a signal at δ 4.84 ppm due to the NH proton. The protons due to the phenyl ring appear as multiplets between 7.60 and 7.11 ppm, and the pyridine ring between 8.86 and 8.19 ppm. The signals at δ 174.62 and 153.88 ppm in the ^{13}C NMR spectrum are attributed to the >C–S (C1) and >C=N (C2) carbons, respectively, of the thiadiazole ring. In the ^{1}H NMR spectrum of [PhHg(ppt)] (**2**), the disappearance of NH proton at 4.84 ppm shows bonding of the deprotonated

Table 1
TD-DFT calculated electronic transitions for the complex [PhHg(ppt)] (**2**).

Excitation energy (eV)	Wavelength (nm)	Oscillator strength	Composition	Major contribution
1.9292	642.66	0.75599	HOMO−1 → LUMO	$\pi \rightarrow \pi^*$
2.8043	442.12	0.60031	HOMO → LUMO+3	$\pi \rightarrow \pi^*$
2.8522	434.70	0.85190	HOMO → LUMO+1	$\pi \rightarrow \pi^*$
3.2103	386.21	0.76996	HOMO−2 → LUMO	$n \rightarrow \pi^*$
3.3943	365.27	0.64257	HOMO−1 → LUMO+1	LMCT
3.4849	355.77	0.68121	HOMO−1 → LUMO+3	LMCT
4.1938	295.64	0.77377	HOMO−1 → LUMO+4	$n \rightarrow \pi^*$
4.3480	285.16	0.99711	HOMO−1 → LUMO+5	$n \rightarrow \pi^*$
4.5591	271.95	0.74963	HOMO−3 → LUMO	LLCT
4.6221	268.24	0.76864	HOMO−4 → LUMO	LLCT

Table 2
TD-DFT calculated electronic transitions for the complex [PhHg(mpcdt)] (**3**).

Excitation energy (eV)	Wavelength (nm)	Oscillator strength	Composition	Major contribution
3.9679	312.47	0.75951	HOMO → LUMO	$\pi \rightarrow \pi^*$
4.3922	282.28	0.58086	HOMO → LUMO+1	$\pi \rightarrow \pi^*$
4.7364	261.77	0.56893	HOMO−1 → LUMO	LLCT
4.8279	256.81	0.68312	HOMO+1 → LUMO+2	$n \rightarrow \pi^*$
4.8780	254.17	0.70516	HOMO−3 → LUMO	ILCT

nitrogen with the phenylmercury(II) cation in complex **2**. The ^{13}C NMR spectrum of complex **2** shows various signals for carbon atoms, of which the signals at δ 174.44 and 150.72 ppm are due to the >C–S and >C=N carbons, respectively. The ^{1}H NMR spectrum of [K(mpcdt)] exhibits three signals at δ 2.20, 3.06 and 4.38 ppm for the methylene and methyl protons of the piperazine ring. In the ^{1}H and ^{13}C NMR spectra of the complex [PhHg(mpcdt)] (**3**), the appearance of signals in the aromatic region suggests complexation of the carbodithioate ligand with the phenylmercury(II) ion. An upfield shift of 2.0 ppm in the CS_2 carbon as compared to the free carbodithioate ligand indicates Hg–S bonding in complex **3**.

3.3. Electronic absorption and photoluminescent properties

The experimentally observed absorption bands of the complexes [PhHg(ppt)] (**2**) and [PhHg(mpcdt)] (**3**) have been explained with the help of TD-DFT calculations. The vertical excitation energies, oscillator strength and tentative nature of the transitions obtained at the TD-DFT level have been presented in Tables 1 and 2. The optimized geometries of the ligands Hppt and [K(mpcdt)], and their complexes [PhHg(ppt)] (**2**) and [PhHg(mpcdt)] (**3**), are shown in Fig. 1. Since each absorption line in a TD-DFT spectrum is due to several single excitations, a depiction of the transition character is generally not straightforward. Calculations indicate that the complex [PhHg(ppt)] (**2**) shows six bands at 642, 434, 365, 355, 271 and 268 nm (experimentally observed at 254, 263 and 351 nm in DMSO solution). Energy bands calculated at 642 and 434 nm with oscillator strengths (*f*) 0.7559 and 0.8519 are due to HOMO−1 → LUMO and HOMO → LUMO+1 electronic excitations, and are attributed to electron transfer from the nitrogen atom of the ligand to the d-orbital of metal ion. The other two bands calculated at 365 and 355 nm with oscillator strengths (*f*) 0.6425 and 0.6812, respectively, are assigned to the charge transfer transitions from the coordinated nitrogen atom and π-electron clouds of the aromatic ring to the metal d-orbital. Additionally, the absorptions calculated at 271 and 268 nm with oscillator strengths (*f*) 0.7496 and 0.7686, respectively, are suggested to be ligand-to-ligand (LLCT) and intraligand (ILCT) charge transfer transitions, which are listed in Table 1 and Fig. 2. In the case of the complex [PhHg(mpcdt)] (**3**), the electronic absorption spectrum displayed three bands at 312, 261 and 254 nm (experimentally observed at 258 and 297 nm in DMSO solution). Quantum chemical calculations reveal that the first lower energy band, calculated at 312 nm with an oscillator strength (*f*) of 0.5903, can be assigned to the HOMO → LUMO electron transfer from the coordinated sulfur atoms of the carbodithioate ligand with a slight intermingling of the metal d-electrons to the aromatic ring. The remaining lower energy bands, calculated at 261 and 254 nm having oscillator strengths of (*f*) 0.5689 and 0.7051, respectively, arise from ligand to ligand (LLCT) and intraligand (ILCT) charge transfers (Table 2 and Fig. 3). The calculated and observed bands are in good agreement for both complexes.

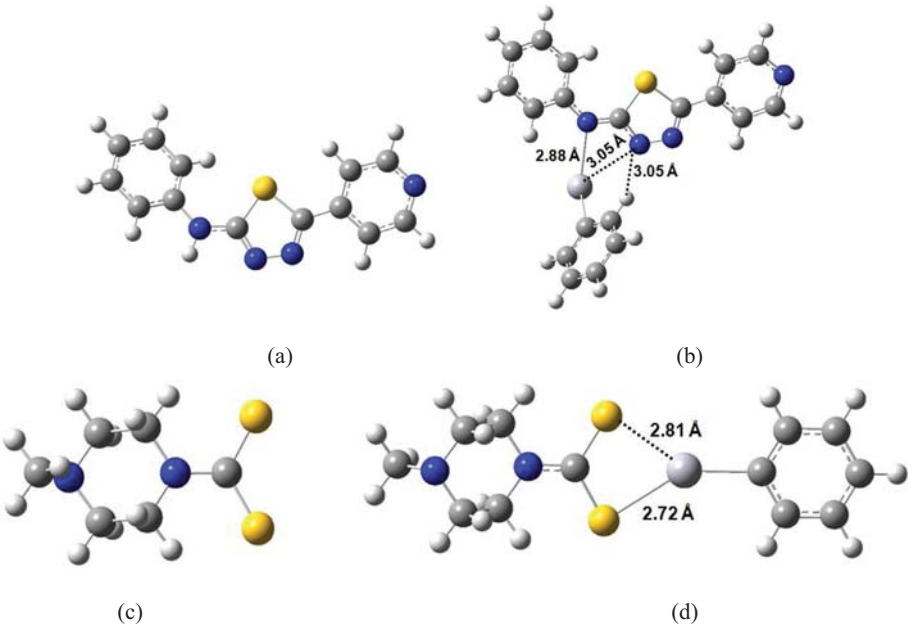

Fig. 1. (a) Optimized geometry of Hppt. (b) Optimized geometry of [PhHg(ppt)]. (c) Optimized geometry of K[mpcdt]. (d) Optimized geometry of [PhHg(mpcdt)].

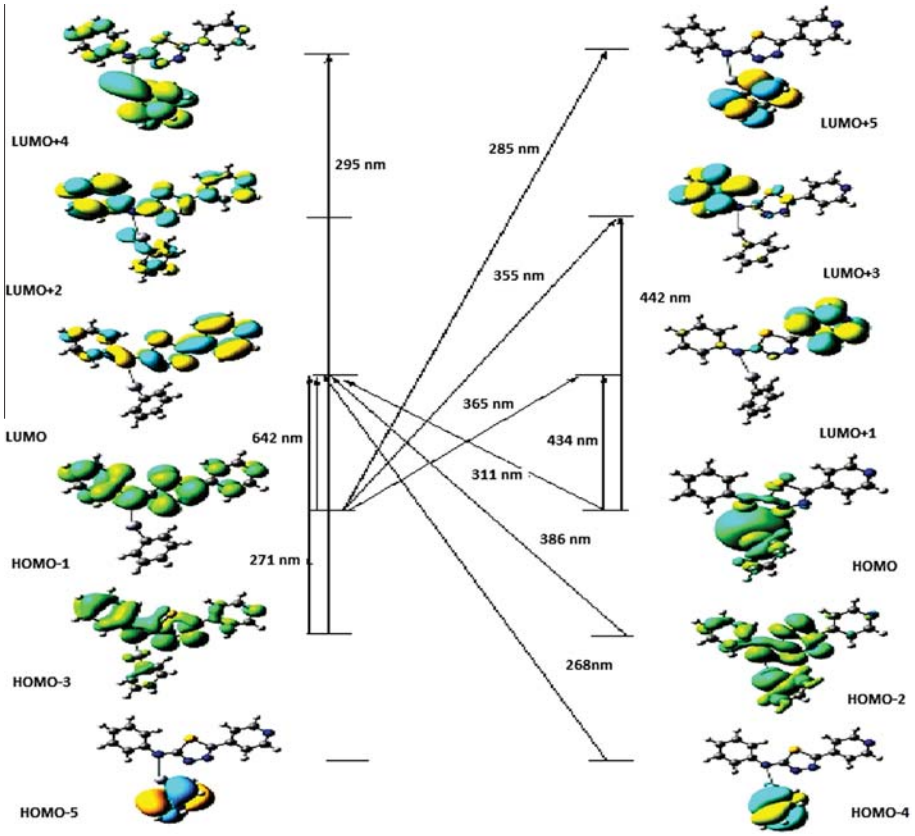

Fig. 2. Electronic transitions of selected molecular orbitals for complex **2**. An isosurface value of 0.02 e/Å^3 was used for the orbitals.

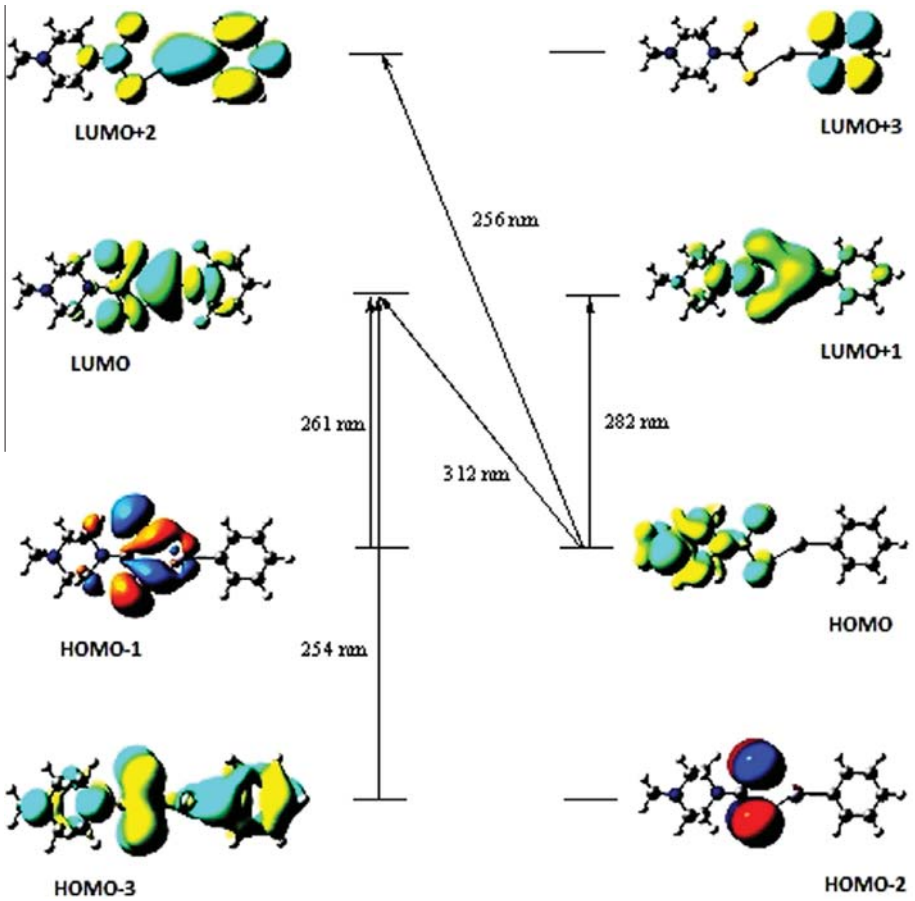

Fig. 3. Electronic transitions of selected molecular orbitals for complex **3**. An isosurface value of 0.02 e/Å^3 was used for the orbitals.

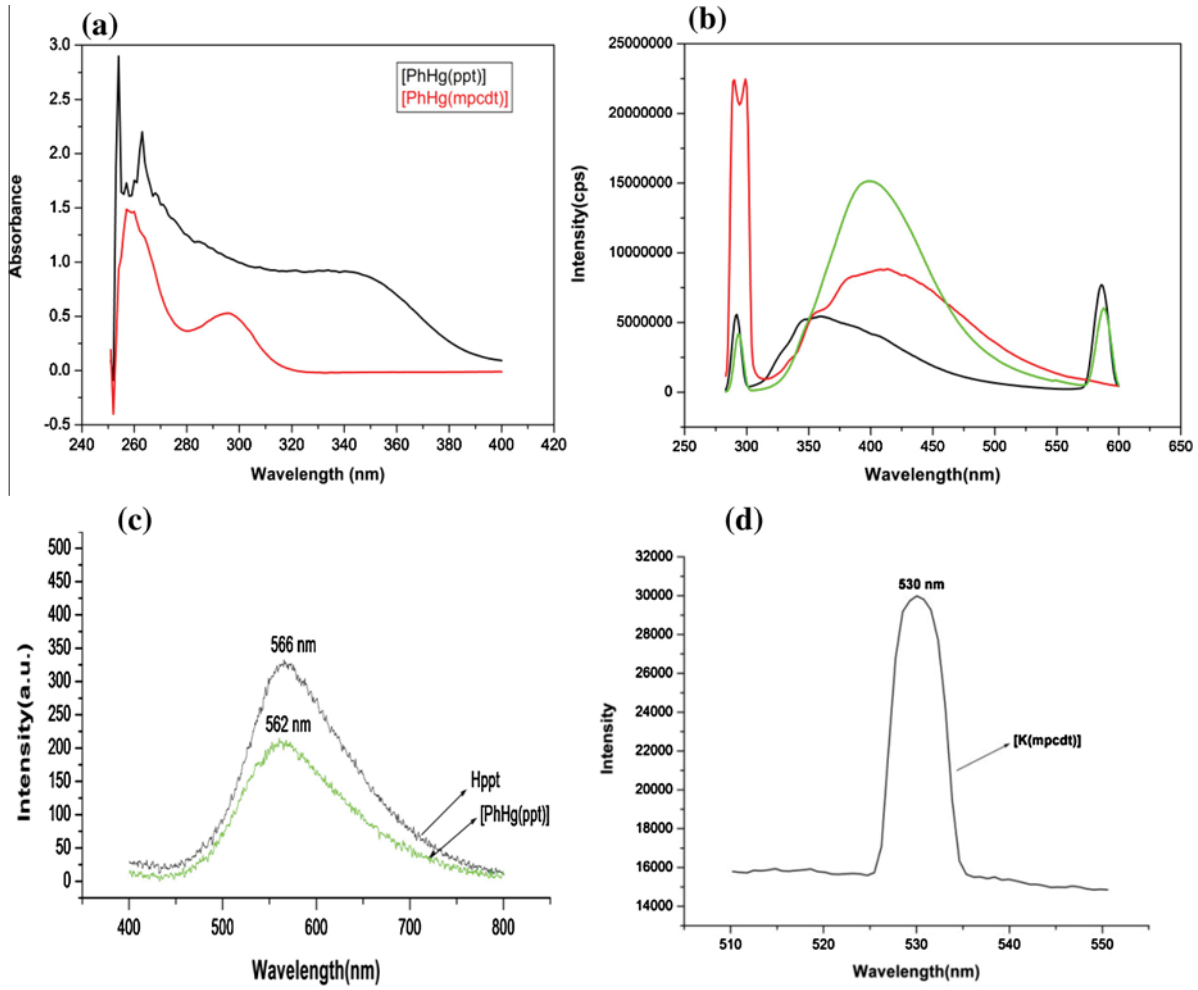

Fig. 4. (a) UV–Vis spectra of [PhHg(ppt)] (**2**) and [PhHg(mpcdt)] (**3**) at 1×10^{-5} M concentration in DMSO solution. (b) The solution state photoluminescent emission spectra of complex **2** at various (1×10^{-3}–1×10^{-5} M) concentrations in DMSO solution. (c) Solid state photoluminescent emission spectra of Hppt and [PhHg(ppt)] (**2**). (d) Solid state photoluminescent emission spectrum of the ligand [K(mpcdt)].

The photoluminescent properties of the ligands Hppt and [K(mpcdt)] and their phenylmercury(II) complexes were examined in the solid state at room temperature (30 °C). The ligands Hppt and [K(mpcdt)] displayed a photoluminescent emission at 566 and 530 nm upon excitation with a 355 and 268 nm laser source. The main chromosphere of the ligand Hppt is the aromatic five-membered thiadiazole ring, and its conjugation degree is further enhanced by the pyridine and phenyl rings. For Hppt, the strong emission is ascribed to an interligand charge transfer transition from the HOMO (π) residing on the phenyl ring to the LUMO (π) localized on the thiadiazole ring, which is further supported by the existence of $\pi\cdots\pi$ interactions in the crystal structure. The complex [PhHg(ppt)] (**2**), on excitation with a 355 nm laser source at room temperature, resulted in a slight blue shift (4 nm) compared to the free ligand Hppt. This is presumably due to a slight decrease of the π electron density on the thiadiazole ring when the ligand coordinates to the phenylmercury cation. Complex **2** exhibits a slightly lower luminescent property as compared to the ligand Hppt, with respect to intensity and energy. The origin of the solid state luminescence emissions of the ligand is suggested to be mainly due to interligand charge transfer transitions (ILCT), but in its complex this is mainly from ligand to metal charge transfer transitions (LMCT). Complex **3** shows no photoluminescence, which indicates that quenching behaviour is observed in this complex. The solution state photoluminescence properties of complex **2** in DMSO indicates that increasing the dilution of solution (1×10^{-3}–1×10^{-5} M) resulted in slight blue shift [15] and a decrease in intensity at various concentrations due to weakening of the $\pi\cdots\pi$ interactions, but the luminescent properties persist even in very dilute solution (Fig. 4) due to the existence of intermolecular as well as intramolecular Hg···N secondary interactions. The green emission of Hppt, [K(mpcdt)] and complex **2** in the solid state implies that these compounds may be potentially applicable as materials for light emitting diode devices [16].

3.4. Electrostatic potential mapping

In order to validate and to understand the complex formation of the ligands with phenyl mercury, molecular electrostatic potential (ESP) mappings were performed. The molecular electrostatic potential (ESP) at a point r in the space around a molecule is given by (in atomic units):

$$V(r) = \sum \frac{Z_A}{|R_A - r|} - \int \frac{\rho(r)(dr')}{|r' - r|}$$

where Z_A is the charge on nucleus A located at R_A and $\rho(r')$ is the electronic density. The first term in the expression represents the effect of the nuclei and the second represents that of the electrons. The electrostatic potential correlates with the dipole moment, electronegativity, partial charges and the site of chemical reactivity of the molecule. It provides a visual method to understand the relative polarity of a molecule. The electron density isosurface on to which

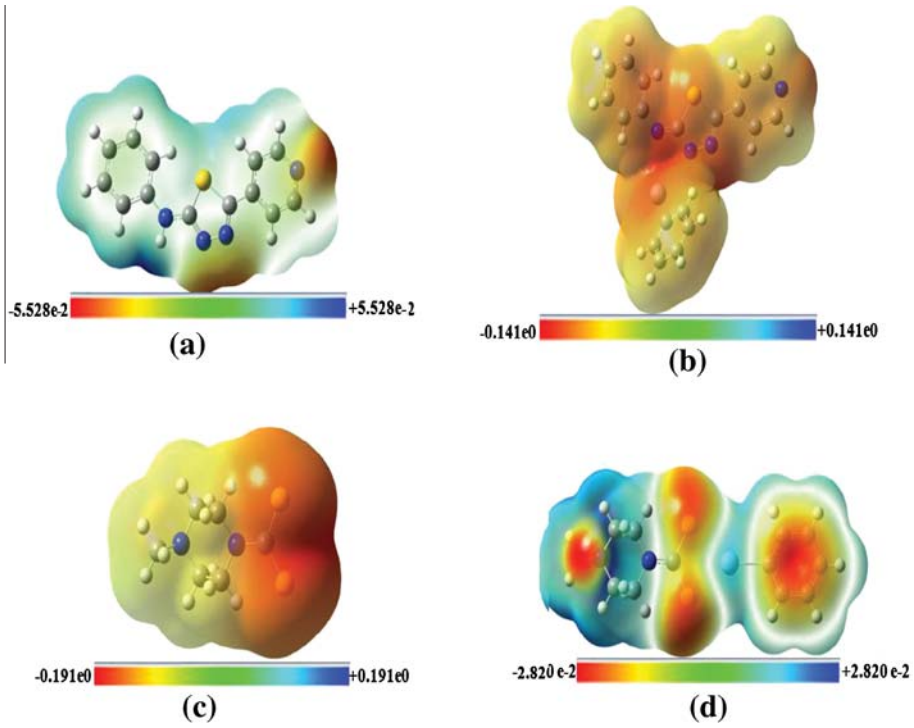

Fig. 5. Electrostatic potential plotted at the van der Waals surfaces for Hppt, [K(mpcdt)] and their complexes **2** and **3**, calculated at the B3LYP level of theory. Red regions – most negative electrostatic potential; blue regions – most positive electrostatic potential; green regions – zero potential. (Colour online.)

Table 3
Crystallographic data for compounds **1**, **2** and **3**.

Parameters	**1**	**2**	**3**
Empirical formula	$C_{13}H_{10}N_4S$	$C_{19}H_{14}HgN_4S$	$C_{12}H_{16}HgN_2S_2$
Formula weight	254.31	531.00	453.00
Crystal system	monoclinic	monoclinic	orthorhombic
Space group	*C*2/*c*	$P2_1/n$	*Pbca*
T (K)	293(2)	293(2)	293(2)
λ, Mo Kα (Å)	0.71073	0.71073	0.71073
a (Å)	27.245(2)	5.0490(9)	7.5586(3)
b (Å)	5.5866(7)	17.817(3)	14.7254(7)
c (Å)	16.5438(13)	18.873(3)	26.2893(12)
α (°)	90.00	90.00	90
β (°)	104.945(6)	95.451(3)	90
γ (°)	90.00	90.00	90
V (Å^3)	3649.7(5)	1690.0(5)	2926.1(2)
Z	8	4	8
$\rho_{calc.}$ (g/cm^3)	1.389	2.087	2.057
μ (mm^{-1})	0.252	9.239	10.786
F(000)	1056	1008	1712
Crystal size (mm)	0.35 × 0.25 × 0.17	0.27 × 0.25 × 0.23	0.23 × 0.21 × 0.19
θ range for data collections (°)	3.08–29.03	2.17–28.47	2.77–32.02
Index ranges	$-36 \leqslant h \leqslant 28$	$-6 \leqslant h \leqslant 6$	$-9 \leqslant h \leqslant \leqslant 11$
	$-6 \leqslant k \leqslant 7$	$-18 \leqslant k \leqslant 23$	$-21 \leqslant k \leqslant 21$
	$-22 \leqslant l \leqslant 22$	$-25 \leqslant l \leqslant 16$	$-39 \leqslant l \leqslant 39$
No. of reflections collected	2883	4272	5076
No. of independent reflections (R_{int})	2124	3116	2816
No. of data/restrains/parameters	2883/0/163	4272/0/179	5076/0/155
Goodness-of-fit on F^2	1.045	1.009	1.000
R_1[a], wR_2[b] [$(I > 2\sigma(I))$]	0.0614, 0.1146	0.0326, 0.0833	0.0442, 0.1386
R_1[a], wR_2[b] (all data)	0.0408, 0.1075	0.0636, 0.1256	0.1020, 0.1704
Largest difference in peak/hole (e Å^{-3})	0.274, −0.161	0.924, −0.645	1.952, −1.492

[a] $R_1 = \sum||F_o| - |Fc||\sum|F_o|$
[b] $R_2 = [\sum w(|F_o^2| - |F_c^2|)^2 / \sum w|F_o^2|^2]^{1/2}$.

the electrostatic potential surface has been mapped is shown in Fig. 5 for the ligands and their complexes with phenyl mercury. Such surfaces depict the size, shape, charge density and site of chemical reactivity of the molecules. The different values of the electrostatic potential at the surface are represented by different colours; red regions – the most negative electrostatic potential, blue regions – the most positive electrostatic potential, and green regions – zero potential. The potential increases in the order

Table 4
Interatomic distances (Å) and angles (°) for Hppt (**1**).

	Expt.	Calc.		Expt.	Calc.
Bond length (Å)			*Bond angles (°)*		
S(1)–C(2)	1.741(16)	1.7762	C(2)–S(1)–C(1)	87.18(7)	85.98
S(1)–C(1)	1.735(14)	1.7552	N(2)–C(1)–N(1)	119.72(13)	120.20
N(1)–C(1)	1.345(19)	1.3639	N(2)–C(1)–S(1)	112.92(11)	110.78
N(1)–C(8)	1.400(19)	1.4061	N(1)–C(1)–S(1)	127.36(12)	125.68
N(3)–C(2)	1.298(19)	1.2983	C(1)–N(2)–N(3)	113.08(12)	112.87
N(3)–N(2)	1.364(18)	1.3520	N(3)–C(2)–C(3)	122.75(15)	121.34
C(1)–N(2)	1.317(19)	1.3140	N(3)–C(2)–S(1)	113.40(12)	114.08
C(3)–C(2)	1.463(2)	1.4641	C(3)–C(2)–S(1)	123.84(11)	121.45

Table 5
Interatomic distances (Å) and angles (°) for [PhHg(ppt)] (**2**).

	Expt.	Calc.		Expt.	Calc.
Bond length (Å)			*Bond angles (°)*		
Hg(1)–C(14)	2.065(13)	2.0320	C(14)–Hg(1)–N(1)	173.0(4)	170.16
Hg(1)–N(1)	2.130(10)	2.1110	C(2)–S(1)–C(1)	87.2(6)	85.60
S(1)–C(2)	1.730(14)	1.7727	C(1)–N(2)–N(3)	112.3(12)	110.08
S(1)–C(1)	1.750(14)	1.8296	C(1)–N(1)–Hg(1)	106.8(8)	92.94
N(2)–C(1)	1.320(18)	1.3595	C(8)–N(1)–Hg(1)	123.8(9)	138.25
N(2)–N(3)	1.343(16)	1.3279	C(15)–C(14)–Hg(1)	122.4(10)	121.09
N(3)–C(2)	1.472(4)	1.3098	C(19)–C(14)–Hg(1)	122.2(10)	121.04

Table 6
Interatomic distances (Å) and angles (°) for [PhHg(mpcdt)] (**3**).

	Expt.	Calc.		Expt.	Calc.
Bond length (Å)			*Bond angles (°)*		
Hg(1)–C(12)	2.070(7)	2.0578	C(12)–Hg(1)–S(1)	165.9(17)	164.06
Hg(1)–S(1)	2.395(17)	2.7000	C(12)–Hg(1)–S(2)	122.2(2)	146.36
Hg(1)–S(2)	3.007(2)	2.8100	S(1)–Hg(1)–S(2)	65.7(5)	63.08
S(1)–C(1)	1.746(7)	1.7428	C(1)–S(1)–Hg(1)	96.3(2)	86.25
S(2)–C(1)	1.691(6)	1.7434	C(1)–S(2)–Hg(1)	77.5(2)	86.36
N(1)–C(1)	1.327(8)	1.3435	C(11)–C(12)–Hg(1)	121.4(5)	120.70
N(1)–C(2)	1.481(8)	1.3980	C(7)–C(12)–Hg(1)	119.6(6)	117.98
N(3)–C(5)	1.463(11)	1.3896	S(2)–C(1)–S(1)	119.9(4)	120.08

red < orange < yellow < green < blue. While the negative electrostatic potential corresponds to an attraction of a proton by the concentrated electron density in the molecule (colours in shades of red), the positive electrostatic potential corresponds to repulsion of a proton by atomic nuclei in regions where low electron density exists and the nuclear charge is incompletely shielded (colours in shades of blue). These ligands contain nitrogen and sulfur atoms and the shape of the electrostatic potential surface is influenced by the charge density distributions in the molecules with sites close to the nitrogen and sulfur showing regions of the most negative electrostatic potential. In the case of the ligands, the N and S atoms are electronegative, so they show the most negative electrostatic potential (very close to red colour). However, in the case of the complexes, a significant amount of charge is redistributed (Fig. 5). In the complex [PhHg(ppt)] (**2**) the electron density is distributed over the molecule homogeneously, while in complex [PhHg(mpcdt)] (**3**) the electron density is mainly concentrated on the nitrogen and sulfur atoms of the carbodithioate ligand and the central part of the phenylmercury cation.

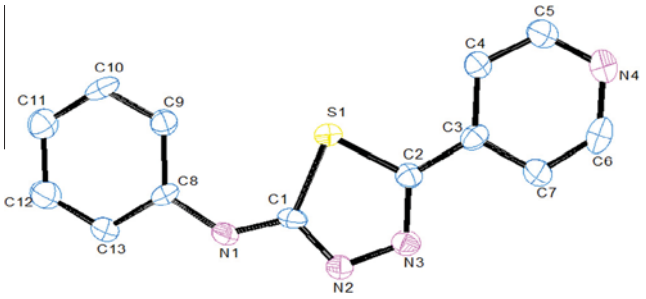

Fig. 6. Ortep diagram of Hppt (**1**) showing the atom numbering scheme. The thermal ellipsoids are plotted at the 30% probability level.

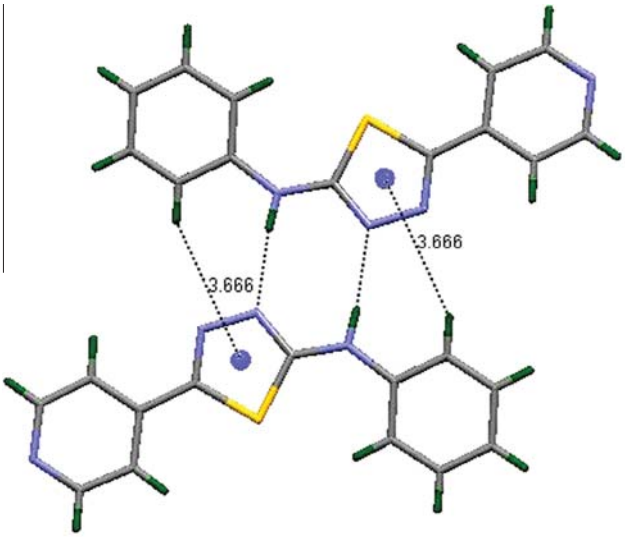

Fig. 7. Showing N–H···N hydrogen bonding and C–H···π interactions leading to the supramolecular structure in **1**.

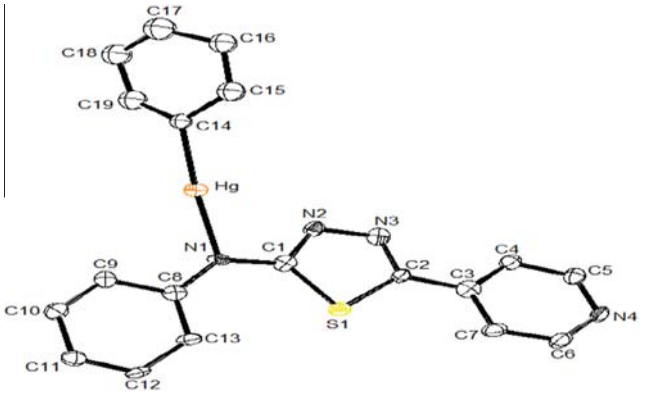

Fig. 8. Ortep diagram of [PhHg(ppt)] (**2**) showing the atom numbering scheme. The thermal ellipsoids are plotted at the 30% probability level.

Table 7
Hydrogen bond parameters [Å and °] in Hppt (**1**).

D–H···A	*d*(D–H)	*d*(H···A)	*d*(D···A)	<(DHA)	Symmetry equivalent operators
N1–H1···N2A	0.859	2.061	2.917	174.07	$2-x, -1-y, 1-z$
N1A–H1A···N2	0.861	2.047	2.903	173.55	$2-x, -1-y, 1-z$

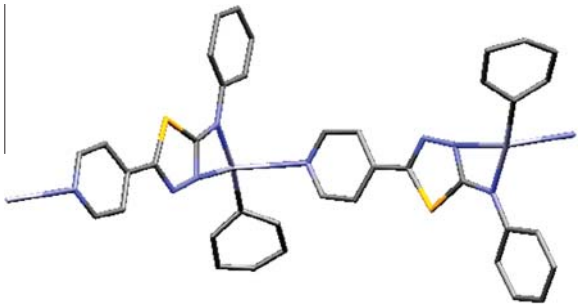

Fig. 9. "Head-to-tail" dimeric structure for **2** displaying weak intramolecular and intermolecular Hg···N secondary interactions.

3.5. Computational details

All the computational calculations were performed using the GAUSSIAN 09 programming package [17]. The geometrical optimization of the ligands and complexes **2** and **3** were calculated in the gas phase using density functional theory (DFT) with the B3LYP hybrid functional for predicting molecular properties [18]. B3LYP is a hybrid functional consisting of Becke's exchange functional, the Lee–Yang–Parr correlation functional and a HF exchange term. It is well known fact that DFT, using a non-local and gradient corrected functional, performs as equally well as other correlated methods, such as calculations at the MP2 level of theory [19]. In studies reported recently [20], DFT calculations with the B3LYP method showed a nice correlation with experimental results and several meaningful conclusions were drawn from those calculations. In the present study, the Lanl2dz basis set [21] was employed for the heavy Hg atom and the 6-311++g(d, p) basis set for the C, H, N and S atom containing molecules in all the calculations. The global minima on the potential energy surface were confirmed by the real harmonic vibrational wavenumbers calculated for each calculated molecular geometry. The optimized structures of the complexes at DFT level were used for molecular orbital analyses and vertical electronic spectra calculations. The electronic excitation energies and intensities of the six lowest-energy spin allowed transitions were calculated using the time dependent density functional theory (TD-DFT). In addition to this, the electrostatic potential mapping surfaces were also plotted for a more clear presentation regarding the charge distributions.

3.6. Crystal structure description

The crystallographic data and structural refinement details for Hppt (**1**), [PhHg(ppt)] (**2**) and [PhHg(mpcdt)] (**3**) are given in Table 3 and selected bond distances and bond angles in Tables 4–6. Hydrogen bond parameters for Hppt (**1**) are given in Table 7.

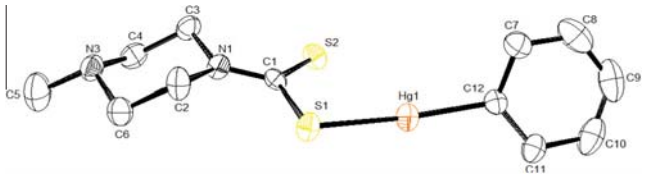

Fig. 11. Ortep diagram of [PhHg(mpcdt)] (**3**) showing the atom numbering scheme. The thermal ellipsoids are plotted at the 30% probability level.

3.6.1. Crystal structure description of Hppt (*1*)

Fig. 6 shows an ORTEP diagram of the ligand Hppt (**1**) together with the atom numbering scheme, and selected bond distances and bond angles are listed in Table 4 along with theoretically predicted data at B3LYP level of theory. The molecular structure of Hppt (**1**) shows that the dihedral angles between the thiadiazole–pyridine and thiadiazole–phenyl rings are 2.05° and 5.06° respectively, indicating that these pairs are almost coplanar to each other. Bond lengths and angles in the pyridine and thiadiazole rings are normal. The endocyclic S(1)–C(1) (1.735(14) Å) and S(1)–C(2) (1.741(16) Å) bond lengths are comparable and are found to be longer than a typical carbon sulfur double-bond, S=C (1.56 Å) [22], which indicates that 1-isonicotinoyl-4-phenyl thiosemicarbazide is converted to the corresponding 1,3,4-thiadiazole. This is further supported by the N(2)–C(1) and N(3)–C(2) bond lengths of 1.317(19) and 1.298(19) Å, which come in the range of N=C double bonds (1.27 Å) [23]. The structure is stabilized by an intermolecular N–H···N interaction between NH of the amine group and the nitrogen of the thiadiazole ring. The values found for the N–H···N interaction are close to the bond distances and bond angles reported earlier [24,25]. In the crystal of Hppt (**1**), inversion dimers are formed via a pair of N–H···N hydrogen bonds. There are two C–H···π interactions (3.366 Å) occurring between CH of a phenyl ring and π electrons of the thiadiazole ring (Fig. 7).

3.6.2. Crystal structure description of [PhHg(ppt)] (*2*)

Fig. 8 shows an ORTEP diagram of the complex [PhHg(ppt)] (**2**) together with the atom numbering scheme, and it shows a monodeprotonated ligand bonded to PhHg(II) via the thiadiazole nitrogen atom. The environment around Hg(II) is almost linear, having a C(14)–Hg–N(1) bond angle of 172.99(4)° and Hg–N(1) bond length of 2.130(10) Å. The dihedral angle between the thiadiazole and pyridine rings is found to be 7.06°, indicating that both rings are almost planar, whilst the dihedral angle of 9.87° between the phenyl and

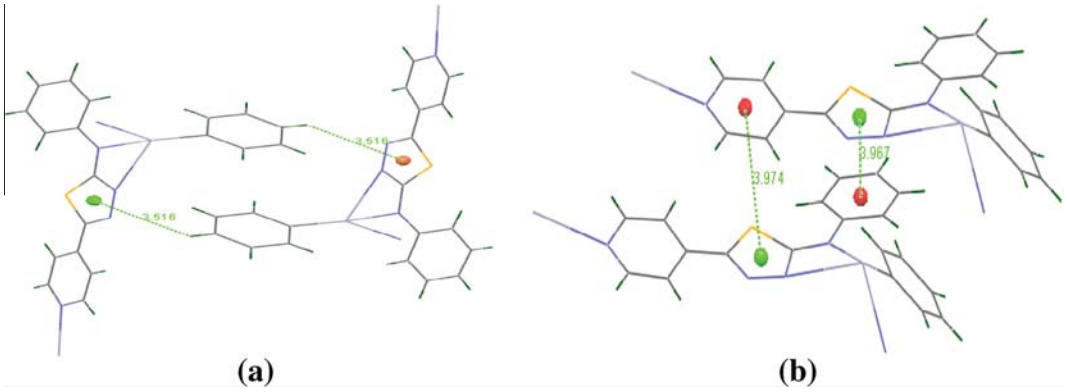

Fig. 10. (a) Showing the C–H···π interaction occurring between a hydrogen of a phenyl ring and π electrons of the thiadiazole ring: (b) weak π···π stacking between pyridine–thiadiazole and phenyl–thiadiazole ring centroids in [PhHg(ppt)] (**2**).

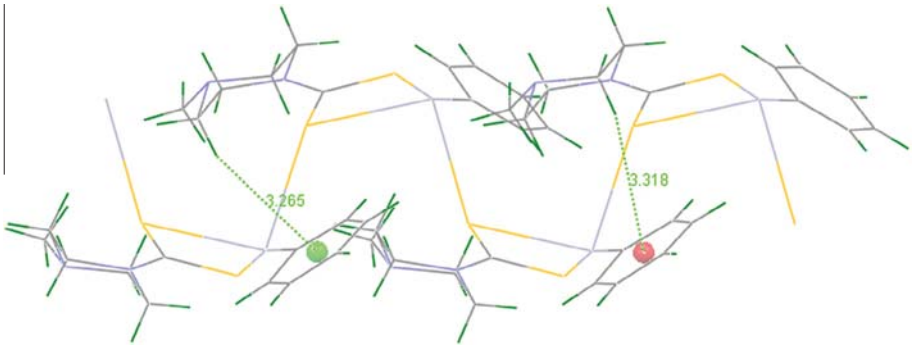

Fig. 12. Two intermolecular C–H···π interactions occurring between a hydrogen atom of a piperazine ring and π electrons of a phenyl ring in [PhHg(mpcdt)] (**3**).

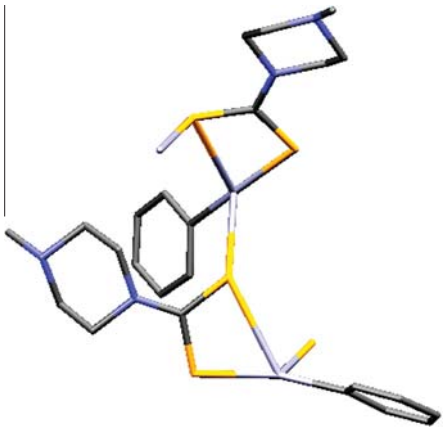

Fig. 13. "Head-to-tail" dimeric structure for **3** displaying weak intramolecular and intermolecular Hg···S secondary interactions.

thiadiazole rings again suggests that both the rings are also coplanar. The dihedral angle between the thiadiazole ring and the phenyl ring attached to mercury is 54.50°, suggesting that the phenyl ring is oriented towards the thiadiazole ring. In complex **2**, there is a weak intramolecular Hg···N_{thia} interaction at a distance of 2.771(9) Å. In addition, complex **2** also contains an intermolecular Hg···N_{Py} secondary interaction at a distance of 2.821(2) Å. Both Hg···N distances are longer than the covalent bond length, but are well within the sum of the van der Waals' radii of the respective elements (r_{vdw}(Hg) = 1.73–2.00 Å and r_{vdw}(N) = 1.55 Å). Intermolecular and intramolecular Hg···N interactions stabilize the structure of the complex (Fig. 9) [26]. The crystal packing of complex **2** shows a weak π···π interaction (3.974 Å) between the phenyl ring and the thiadiazole ring of a nearby molecule (Fig. 10a) [27]. The geometry and bonding parameters agree with those of other related phenylmercury complexes [7,28]. In addition, the structure is stabilized by a C–H···π interaction (3.516 Å) between CH of a phenyl ring and π-electrons of a thiadiazole ring of another unit of the complex (Fig. 10b). To get a clear picture of the binding site and geometry we have performed geometry optimization for complex **2** at the B3LYP density functional theory level. The computed optimized structure of **2** corroborates the geometrical parameters obtained from the crystal structure analysis (Table 5). The results are therefore strongly supported by the present theoretical predictions.

*3.6.3. Crystal structure description of [PhHg(mpcdt)] (**3**)*

Fig. 11 shows the ORTEP diagram of the complex [PhHg(mpcdt)] (**3**) together with the atom numbering scheme. The geometry optimization of complex **3** at the B3LYP level of theory revealed that the bond distances and bond angles are in very good agreement with the experimental data (Table 6). The complex [PhHg(mpcdt)] (**3**) contains a monodeprotonated ligand which is coordinated to the metal via the dithio sulfur atom, and the geometry around Hg(II) is linear. The coordination environment around Hg(II) is fulfilled by the ipso-C atom of the phenyl group and the S(1) atom of the carbodithioate ligand. The C–S bond distances of 1.746(7) and 1.691(6) Å (Table 6) in complex **3** agree well with those in other related compounds, being intermediate between C–S single (1.82 Å) and C=S double (1.56 Å) bond distances [22]. The dihedral angle between the piperazine ring and phenyl ring attached to mercury is found to be 63.61° indicating that the phenyl ring is oriented towards the piperazine ring. The Hg–S(1) bond length is 2.395(17) Å, whilst that of Hg–S(2) is 3.007(2) Å, which suggests a weaker interactions between Hg and S(2), thereby reflecting the propensity of Hg(II) to exist in a linear coordination. The proximity of the atom S(2) is partly responsible for the deviation from the ideal linear geometry, as seen in the (Ph)C–Hg–S(1) bond angle of 165.91(17)°. The bond length and angle are in close agreement with those reported for other similar compounds, with a greater deviation from linearity than in complex **3** [7,28]. This may be attributed to the somewhat weaker intermolecular Hg···S secondary interaction. There are two intermolecular C–H···π interactions (3.265 and 3.318 Å) occurring between CH of piperazine and π electrons of a phenyl ring (Fig. 12). The crystal structure is further stabilized by weak intermolecular and intramolecular Hg···S interactions occurring between the dithio sulfur atom and Hg(II) (Fig. 13). Within the carbodithioate moiety, the C–N bond length of 1.326(3) Å indicates substantial delocalization of the π-electron density [29].

4. Conclusions

This paper reports on the syntheses and crystal structures of two novel complexes, [PhHg(ppt)] (**2**) and [PhHg(mpcdt)] (**3**), of N-phenyl-5-(pyridin-4-yl)-1,3,4-thiadiazol-2-amine (Hppt) (**1**) and potassium N′(4-methylpiperazine)-1-carbodithioate [K(mpcdt)]. It has been observed that the replacement of an aliphatic or aromatic hydrocarbon moiety by a heteroaromatic group such as pyridine makes the ligand able to bind with PhHg(II) thiadiazole via new secondary Hg···N interactions. PhHg(II) carbodithioate involves a new secondary Hg···S interaction. The crystal structures of the ligand **1** and complexes **2** and **3** are stabilized by C–H···π interactions. In addition, complex **2** is stabilized by weak π···π interactions. The solid state photoluminescent properties indicated that the presence of Hg···S interactions quenches the chances of photoemission, whereas a Hg···N_{Py} intermolecular interaction retains or increases the probability. The electronic excitation energies and intensities of the lowest-energy spin allowed transitions were calculated using time dependent density functional theory (TD-DFT) and they were found to match the experimental results, with just slight deviations.

The electrostatic potential mapping surfaces plotted, regarding the charge distributions, indicated a redistribution of charge from the ligand to the metal in the complexes.

Acknowledgements

A. Bharti thanks CSIR, New Delhi for the award of a JRF and Dr. M.K. Bharty is thankful to the Department of Science and Technology, New Delhi, India for the award of a Young Scientist Project (No. SR/FT/CS-63/2011).

Appendix A. Supplementary data

CCDC 786907, 786908, and 875786 contains the supplementary crystallographic data for Hppt (**1**), [PhHg(ppt)] (**2**) and [PhHg(mpcdt)] (**3**), respectively. These data can be obtained free of charge via http://www.ccdc.cam.ac.uk/conts/retrieving.html, or from the Cambridge Crystallographic Data Centre, 12 Union Road, Cambridge CB2 1EZ, UK; fax: (+44) 1223-336-033; or e-mail: deposit@ccdc.cam.ac.uk.

References

[1] T.W. Clarkson, L. Magos, Crit. Rev. Toxicol. 36 (2006) 609.
[2] R.E. Hoffmeyer, S.P. Singh, C.J. Donan, A.R.S. Ross, R.J. Hughes, I.P. Pickering, G.N. George, Chem. Res. Toxicol. 19 (2006) 753.
[3] (a) J.P.K. Rooney, Toxicology 234 (2007) 145;
(b) J.P.K. Rooney, Toxicology 238 (2007) 216.
[4] (a) A.M. Bond, A.R. Hendrickson, R.L. Martin, J.E. Moir, D.R. Page, Inorg. Chem. 22 (1983) 3440;
(b) N. Robertson, L. Cronin, Coord. Chem. Rev. 227 (2002) 93;
M. Bousseau, L. Valade, J. Am. Chem. Soc. 108 (1986) 1908;
(d) A.T. Coomber, D. Beljonne, R.H. Friend, J.L. Bredas, A. Charlton, N. Robertson, A.E. Underhill, Nature 380 (1996) 144;
(e) N. Singh, A. Kumar, Synth. Met. 158 (2008) 442.
[5] (a) E. Wehman, G. van Koten, J.T.B.H. Jastrzebski, J. Chem. Soc., Dalton Trans. (1988) 2975;
(b) A.F.M.J. van der Ploeg, G. van Koten, K. Vrieze, J. Organomet. Chem. 222 (1981) 115.
[6] (a) R.C. Larock, Angew. Chem., Int. Ed. 17 (1978) 27;
(b) J.G. Melnick, K. Yurkerwich, G. Parkin, Inorg. Chem. 48 (2009) 6763.
[7] (a) C.S. Lai, E.R.T. Tiekink, CrystEngComm 5 (2003) 253;
(b) N. Singh, A. Kumar, K.C. Molloy, M.F. Mahon, Dalton Trans. (2008) 4999;
(c) N. Singh, A. Kumar, R. Prasad, K.C. Molloy, M.F. Mahon, Dalton Trans. 39 (2010) 2667;
(d) V. Singh, R. Chauhan, A. Kumar, L. Bahadur, N. Singh, Dalton Trans. 39 (2010) 9779.
[8] (a) M.I. Bruce, B.C. Hall, B.W. Skeleton, M.E. Smith, A.H. White, J. Chem. Soc., Dalton Trans. (2002) 995;
(b) P. Li, B. Ahrens, K.-H. Choi, M.S. Khan, P.R. Raithby, P.J. Khan, M.S. Wilson, W.-Y. Wong, CrystEngComm 4 (2002) 405.
[9] J.S. Casas, Polyhedron 18 (1999) 187.
[10] R. Dulare, S.K. Kushawaha, M.K. Bharty, N.K. Singh, J. Mol. Struct. 984 (2010) 96.
[11] G.M. Sheldrick, Acta Crystallogr. A64 (2008) 112.
[12] C.F. Macrae, I.J. Bruno, J.A. Chisholm, P.R. Edgington, P. McCabe, E. Pidcock, L. Rodriguez-Monge, R. Taylor, J. van de Streek, P.A. Wood, J. Appl. Crystallogr. 41 (2008) 466.
[13] L.J. Farrugia, J. Appl. Crystallogr. 45 (2012) 849.
[14] G.S. Patricia, G.T. Javier, A.M. Miguel, J.A. Francisco, R. Teofilo, Inorg. Chem. 41 (2002) 1345.
[15] (a) L. Szalay, G.S. Singhal, E. Tombacz, L. Kozma, Acta Phys. Acad. Scient. Hung. Tomus 34 (1973) 341–350;
(b) L. Zhu, C. Yang, J. Qin, Chem. Commun. (2008) 6303.
[16] (a) A. Barbieri, G. Accorsi, N. Armaroli, Chem. Commun. (2008) 2185;
(b) S.L. Zheng, X.M. Chen, Aust. J. Chem. 57 (2004) 703.
[17] M.J. Frisch, G.W. Trucks, H.B. Schlegel, G.E. Scuseria, M.A. Robb, J.R. Cheeseman, G. Scalmani, V. Barone, B. Mennucci, G.A. Petersson, H. Nakatsuji, M. Caricato, X. Li, H.P. Hratchian, A.F. Izmaylov, J. Bloino, G. Zheng, J.L. Sonnenberg, M. Hada, M. Ehara, K. Toyota, R. Fukuda, J. Hasegawa, M. Ishida, T. Nakajima, Y. Honda, O. Kitao, H. Nakai, T. Vreven, J.A. Montgomery, J.E. Peralta, F. Ogliaro, M. Bearpark, J.J. Heyd, E. Brothers, K.N. Kudin, V.N. Staroverov, R. Kobayashi, J. Normand, K. Raghavachari, A. Rendell, J.C. Burant, S.S. Iyengar, J. Tomasi, M. Cossi, N. Rega, N.J. Millam, M. Klene, J.E. Knox, J.B. Cross, V. Bakken, C. Adamo, J. Jaramillo, R. Gomperts, R.E. Stratmann, O. Yazyev, A.J. Austin, R. Cammi, C. Pomelli, J.W. Ochterski, R.L. Martin, K. Morokuma, V.G. Zakrzewski, G.A. Voth, P. Salvador, J.J. Dannenberg, S. Dapprich, A.D. Daniels, Ö. Farkas, J.B. Foresman, J.V. Ortiz, J. Cioslowski, D.J. Fox, GAUSSIAN 09, Gaussian, Inc., Wallingford, CT, 2009.
[18] (a) A.D. Becke, Phys. Rev. A 38 (1988) 3098;
(b) A.D. Becke, J. Chem. Phys. 98 (1993) 5648;
(c) H.L. Schmider, A.D. Becke, J. Chem. Phys. 108 (1998) 9624.
[19] M.A. McAllister, THEOCHEM 427 (1998) 39.
[20] (a) D.K. Singh, B.P. Asthana, S.K. Srivastava, J. Mol. Model. 18 (2012) 3541;
(b) D.K. Singh, S.K. Srivastava, B.P. Asthana, Chem. Phys. 380 (2011) 24;
(c) D.K. Singh, S.K. Srivastava, S. Schlucker, R.K. Singh, B.P. Asthana, J. Raman Spectrosc. 42 (2011) 851;
(d) S. Singh, D.K. Singh, S.K. Srivastava, B.P. Asthana, Z Phys. Chem. I (225) (2011) 723–740;
(e) S. Singh, D.K. Singh, S.K. Srivastava, B.P. Asthana, Vib. Spectrosc. 56 (2011) 26.
[21] (a) S. Sardonic, H. Pir, Spectrochim. Acta, Part A 73 (2009) 181;
(b) Y.A. Borisov, A.S. Peregudov, J. Struct. Chem. 44 (2003) 567.
[22] Ram. Dulare, Polyhedron 30 (2011) 1960.
[23] X.Z. You, Progress in Coordination Chemistry, Higher Education Publishing Company, Beijing, 2000.
[24] N.K. Singh, A.K. Pandey, M. Singh, M.K. Bharty, R.J. Butcher, Acta Crystallogr. E63 (2007) 04327.
[25] J.P. Jaisinski, M.K. Bharty, N.K. Singh, S.K. Kushawaha, R.J. Butcher, J. Chem. Crystallogr. 41 (2011) 6.
[26] X.Y. Tang, R.X. Yuan, Z.G. Ren, H.X. Li, Y. Zhang, J.P. Lang, Inorg. Chem. 48 (2009) 2639.
[27] C. Janiak, J. Chem. Soc., Dalton Trans. (2000) 3885.
[28] V. Singh, A. Kumar, R. Prasad, G. Rajput, M.G.B. Drew, N. Singh, CrystEngComm 13 (2011) 6817.
[29] K.A. Wheeler, B. Harrington, M. Zapp, E. Casey, CrystEngComm 5 (2003) 337.